X-ray-absorption spectroscopy in $CoSi_2$ and $NiSi_2$: Experiment and theory

P. Lerch and T. Jarlborg

*Département de Physique de La Matière Condensée, Université de Genève, 24 Quai Ernest-Ansermet,
CH-1211 Genève 4, Switzerland*

V. Codazzi and G. Loupias*

*Laboratoire de Minéralogie-Cristallographie, Université Paris VI et VII, 4 place Jussieu,
75252 Paris CEDEX 05, France*

A. M. Flank

*Laboratoire d'Utilisation du Rayonnement Electromagnétique, Université de Paris–Sud, Bâtiment 209c,
91405 Orsay CEDEX, France*

This paper presents an experimental and theoretical study of x-ray-absorption spectroscopy near the edge. We measured K edges for all atom types and $L_{2,3}$ edges for Co and Ni. Theoretical spectra from a linear-muffin-tin-orbitals band-structure calculation are shown. The effect of the core hole on threshold energies and absorption spectra has been studied. We also show the distribution of the photoelectron in the elementary cell. Threshold energies obtained by using the difference-self-consistent-field method are compared to experimental values. Polarization energies, due to rearrangement of the core orbitals, have been estimated for the different core holes.

I. INTRODUCTION

Transition-metal disilicides have been extensively studied, both theoretically[1-11] and experimentally.[12-17] Among them, $CoSi_2$ and $NiSi_2$ present many interesting features for microelectronics. $CoSi_2$ has become the most used material in metal-silicon-metal transistor technology. It can be epitaxially grown on the Si(111) plane because of the nearly perfect lattice matching between $CoSi_2$ and Si. It has also found applications for gate electrodes and Schottky barriers.

These applications have stimulated a lot of theoretical work. There have been several band-structure (BS) calculations.[1-9] Results of our linear-muffin-tin-orbitals (LMTO) calculation have partly been published earlier.[18] Our calculation is in fair agreement with the LMTO BS of Lambrecht, Christensen, and Blöch[8] and with other self-consistent band structures. The BS approach has been supported by various experiments. Many photoemission measurements have been carried out.[12-17] The photoemission spectra revealed that the metallic character of these compounds results from s- and p-like free electrons, rather than from d electrons as in the metal. A recent positron-annihilation study by Garreau et al.[18] showed good agreement between calculated and measured two-dimensional angular correlation of positron-annihilation radiation. The calculated Fermi surface agrees with de Haas–van Alphen experiments of Newcombe and Lonzarich.[19] Recently, Jia et al.[20] and Nakamura et al.[21] performed soft-x-ray-emission studies on $CoSi_2$ and $NiSi_2$.

The above-mentioned methods probe essentially the occupied states while x-ray-absorption spectroscopy (XAS) is an appropriate experimental method to probe the band states above the Fermi level (E_F). We can select a specific atom type by choosing an energy range corresponding to one of its core levels, and probe band states with the l values permitted by the selection rules. It gives spectra with high resolution, depending on the core level that is considered, and allows for selecting partial density of states (DOS). Moreover, XAS gives not only the shape of the distribution but also the absolute value of the threshold energy. XAS experiments have already been carried out for the K edge of Si in the $3d$ transition-metal disilicides.[22] In this work we studied K and $L_{2,3}$ edges for Co and Ni and Si K edges.

In addition to our experiments, we calculated the XAS spectra within the local-density approximation. The measured XASs are compared to the DOS functions multiplied by the matrix element. We tested different methods to take into account relaxation effects due to the presence of the core hole. Agreement between theory and experiment is extensively discussed for threshold values and spectra structures.

II. EXPERIMENTAL METHOD

The samples were made using a very thin crushed material deposited on a millipore substrate. The K edges were measured in the transmission mode. In this mode, the samples have to be thick enough to absorb 90% of the incident beam, in order to optimize the accuracy; this condition leads to typical thicknesses of 20 μm for the K metal edges (21 μm for Co and 25 μm for Ni) and 1.3 μm for the K edge of Si. The materials are crushed to obtain very thin powder compared to the sample thickness in order to get homogeneous samples after deposition on a millipore substrate.

The thickness required for $L_{2,3}$ edges was too small (10 nm) to allow working in the transmission mode. There-
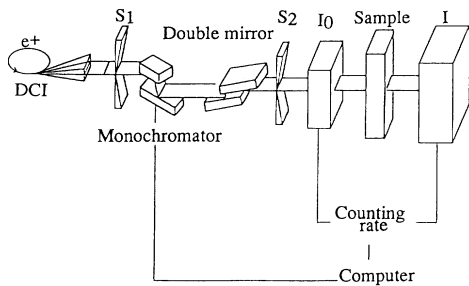
FIG. 1. Experimental setup on the EXAFS II station. As we worked in the transmission mode, the intensity of the x-ray beam is measured before and after having passed through the sample. The ratio of the intensities before and after the sample determines the absorption value for the selected energy.

fore we performed our experiments in the total yield mode. A special effort was made to optimize the experiments, both in the sample preparation and in the choice of the different monochromators. This is necessary to avoid noisy data acquisition and to get highly resolved spectra.

The data edges were recorded at Laboratoire d'Utilisation du Rayonnement Electromagnétique (LURE). We worked on the two synchrotron storage rings of LURE: the K edges of the metals (Co and Ni) were measured at DCI (storage ring of higher energy), on the EXAFS II station, whereas the silicon K edges and the metal $L_{2,3}$ edges were measured at Super-ACO, on the SA 72 station.

In Fig. 1 we present the experimental setup of the EXAFS II station. For the two modes of experiments, a double monochromator provides an x-ray beam tunable around the energy of the studied edge. The monochromator was equipped with the Si(511) reflection for the measurements of Co and Ni K edges. Two uncoated glass mirrors were used to reject the remaining harmonics of the beam. The experimental resolution is determined by the opening of slits S_1 and S_2, their separation, and the size of the source.[23] The overall instrumental resolution is evaluated to be respectively 1.28 eV for Co and 1.64 eV for Ni. The spectra of the photons transmitted were recorded in the energy range 7660–7860 eV for Co, and 8280–8480 eV for Ni, both by steps of 0.3 eV.

On Super-ACO, the principle of the instrumental setup is the same. The difference is that we work under vacuum and the experimental station has no slits and mirrors. We have chosen a specific crystal reflection for the different measurements, in order to optimize the resolution. Thus, three kinds of double crystal were used: InSb (Si K edge) and potassium acid phthalate (KAP) as the second crystal for the Co $L_{2,3}$ edge (a multilayered system is used instead of the first crystal for thermal reasons), and beryl $[Be_3Al_2(SiO_3)_6]$ for the Ni $L_{2,3}$ edge. The instrumental resolution was respectively 0.7, 0.9, and 0.3 eV.[24]

III. THEORETICAL APPROACH

There are three different approaches to compute x-ray-absorption spectra: the band-structure (BS) ap-

proach, the scattering, and the Green's-function approach. All of them are, in principle, equivalent[25] although they are mostly applied to different energy ranges. The scattering formalism considers a central atom and takes into account the neighboring atoms via backscattering waves. This approach is used to compute extended x-ray-absorption fine structure (EXAFS). On the other hand, the BS approach is used to compute the x-ray-absorption near-edge spectra (XANES) or the emission spectra.[26,27] Here we used the BS approach since we are considering the near-edge absorption spectra, i.e., up to nearly 30 eV above E_F. This method to compute XANES has already been successfully applied to describe K and $L_{2,3}$ edges of different materials, among them $3d$ transition-metal disilicides.[22,28]

### A. LMTO band-structure calculation

The self-consistent linear-muffin-tin-orbital (LMTO) method[29] with the local-density approximation (LDA) for exchange and correlation[30,31] has been used. The slight overlapping of the atomic spheres is corrected by the so-called combined correction term. The structures of $CoSi_2$ and of $NiSi_2$ (Refs. 8 and 32) are of fluorite type, the prototype of which is CaF_2. In order to obtain a good space filling an empty sphere was included in each elementary cell. The resulting structure has a fcc lattice with a metal atom centered in $(0,0,0)$, two Si atoms at $(\frac{1}{4},\frac{1}{4},\frac{1}{4})$ and $(\frac{3}{4},\frac{3}{4},\frac{3}{4})$, and an empty sphere at $(\frac{1}{2},\frac{1}{2},\frac{1}{2})$. The experimental value for the lattice parameter is 5.365 Å for $CoSi_2$ and 5.41 Å for $NiSi_2$.[32] The radii of the atomic spheres were assumed equal for the metal and Si atoms and smaller for the empty site in order to avoid charge localization inside this sphere.

We included s, p, and d waves for both metal and Si atoms on each site and f tails coming from neighboring atoms. For the empty sphere the expansion goes up to p waves with d tails coming from other sites. Core functions are fully relativistic and not frozen in order to achieve self-consistency, while all relativistic effects are included, except for the spin-orbit coupling for the valence states. We used 89 k points in the irreducible Brillouin zone (IBZ). The DOS were calculated with 505 k points in the IBZ using a tetrahedron integration method.[33]

There have been several previous calculations of $CoSi_2$ (Refs. 3–5 and 7–9) and $NiSi_2$ (Refs. 1–6 and 8) band structures. The topology of the Fermi surface, which has been discussed elsewhere,[9,18] consists essentially of three nested hole sheets at the Γ point. In Fig. 2, we show the partial DOS for both disilicides. The Fermi surface and other aspects of the band structure of $CoSi_2$ have been published earlier together with a study of positron annihilation.[18]

B. X-ray-absorption spectra

Let us consider a core level $c = (n,l,j)$ with an energy ε_c and a wave function ϕ_c. Then the resulting absorption due to transitions from this core state to different band states $\phi_{K,j}$ (where j labels different bands) above the Fer-

CoSi₂

NiSi₂

Energy relative to E_F (eV)
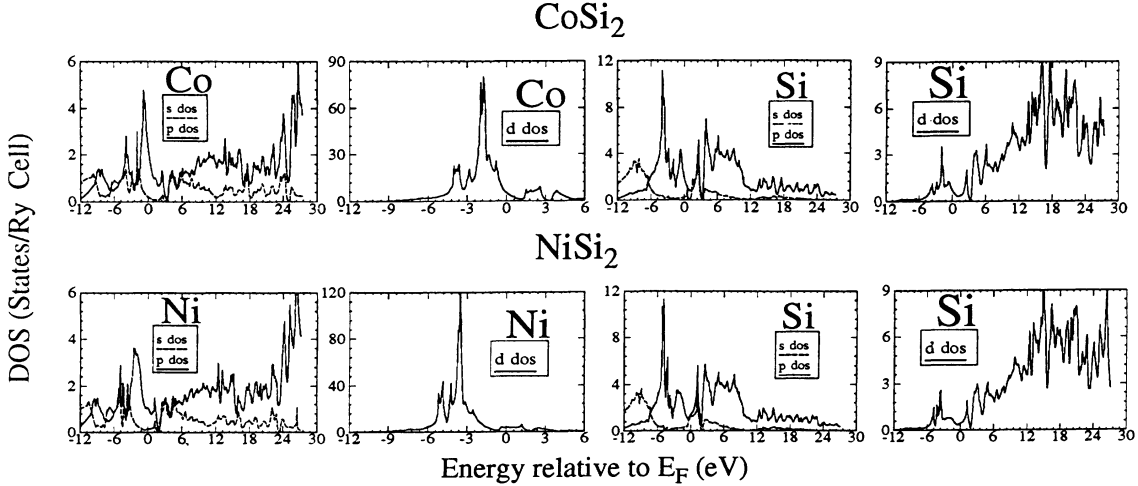
FIG. 2. Partial DOSs for CoSi₂ and NiSi₂.

mi energy (E_F) can be written as[34]

$$\mu_c(E) = \frac{4\pi^2 e^2 \nu}{3c\hbar\Omega}(E - \varepsilon_c) \sum_{K,j} |\langle \phi_c | \mathbf{r} | \phi_{Kj} \rangle|^2 \delta(E - E_{K,j})$$

$$(E > E_F) \ , \quad (1)$$

where ν is the number of contributing atoms in the primitive cell and Ω is the volume of this cell. This expression contains two approximations. First, the dipole approximation which is justified since we are dealing with rather light elements.[34] Second, we consider a polycrystalline sample; this allows us to take the spherical average over the polarization vector $\boldsymbol{\epsilon}$ of the x-ray beam:

$$\overline{|\langle \phi_c | \boldsymbol{\epsilon} \cdot \mathbf{r} | \phi_{Kj} \rangle|^2} = \tfrac{1}{3} |\langle \phi_c | \mathbf{r} | \phi_{Kj} \rangle|^2 \ . \quad (2)$$

With these approximations the spectra can be factorized into a matrix element (giving the probability of the dipolar transition to the various empty band states) multiplied by the density of band states with angular momentum satisfying dipolar selection rules. In the case of K edges, this factorization leads to

$$\mu_K(E) = \frac{4\pi^2 e^2 \nu}{9c\hbar\Omega}(E - \varepsilon_c) r_p^2(E) N_p(E) \ ; \quad (3)$$

whereas for L_2 or L_3 edges,

$$\mu_L(E) = \frac{4\pi^2 e^2 \nu}{3c\hbar\Omega}(E - \varepsilon_c)[r_s^2(E)N_s(E) + \tfrac{2}{5}r_d^2(E)N_d(E)] \ , \quad (4)$$

where $N_l(E)$ is the nonoccupied DOS of l character on the same site as ϕ_c. For the L_2 spectra, the matrix elements r_s and r_d have to be computed with the $2p_{1/2}$ core state, while for L_3 spectra we consider a $2p_{3/2}$ core state. The $L_{2,3}$ edge is finally the sum of L_2 and L_3 spectra. The threshold of the two spectra is separated by the spin-orbit energy. Essentially, identical expressions as Eqs. (1)–(4) can be adopted for calculations of soft x-ray emission spectra, which are probes of the occupied DOS functions.[27] It should be noted that $(E - \varepsilon_c)$ is much

larger than the energy range for which we usually calculate $\mu(E)$, so the prefactor $(E - \varepsilon_c)$ can be considered as constant. The matrix elements are computed for the different normalized core states ϕ_C with the radial part R_c:

$$r_l(E) = \langle R_c | \mathbf{r} | R_l(E) \rangle \ . \quad (5)$$

Here $R_l(E)$ is the normalized radial wave function with angular momentum l and energy E in the self-consistent potential obtained from the band-structure calculation. The matrix elements are atomiclike in the sense that only the localized part of $R_l(E)$ contributes, since the core functions are very localized. To compute the matrix elements, the integration is performed up to the Wigner-Seitz (WS) radius of the atom considered. It should be noted that the energy dependence of r_l^2 is only smooth, so that the fine structures into the XANES enter via the local DOS functions. However, for $L_{2,3}$ edges, the relative strength between s-p and d-p matrix elements is crucial for the projection of s or d DOS in the XANES process.

C. Matrix elements

The matrix elements for different transitions are shown in Fig. 3. For K edges we consider transitions to p states; the matrix element is increasing with energy. This results from a better overlapping of the $1s$ core function with p states of higher energies (which are more localized at the top of the band region), since due to normalization the amplitude of the p states increase at small r. However, it does not affect the main characteristics of K-edge spectra. In the case of $L_{2,3}$ edges, starting with $2p_{1/2}$ and $2p_{3/2}$ core states, transitions to both s and d states have to be considered.

For Co and Ni, transitions to d states are much more probable than to s states. As the XANES depends upon the square of the matrix element, the spectra are dominated by the d DOS. In the case of Si, s and d matrix elements are of comparable magnitude and the absorption spectra contain features of both s and d DOSs.
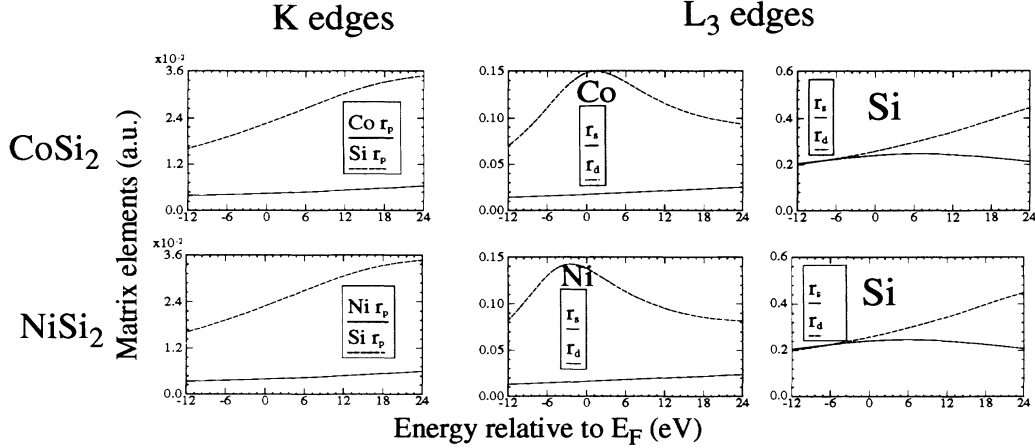
K edges

L₃ edges

FIG. 3. Calculated matrix elements for K and L_3 edges for both metal and Si atoms in $CoSi_2$ and $NiSi_2$. For K edges there are transitions to p band states, while transitions to s and d band states are allowed for the L_3 edge. As is seen from the figure, transitions to d states largely dominate the L_3 edge for Co and Ni.

D. Density of states

Partial DOSs are shown in Fig. 2. The main feature of Co and Ni partial DOSs is their strong peak due to their flat (dispersion of 1 eV) $3d$ bands. This peak is localized well below E_F. Nevertheless, these d states extend above E_F and they determine the $L_{2,3}$ edges. There are two peaks just above E_F, which is favorable for a precise determination of the threshold energy.

The metallic character of these disilicides results merely from s- and p-like quasi free electrons at the Si site. Of interest is the p DOS since it determines the absorption spectra for the K edges. For Co and Ni, p DOS is smoothly increasing with energy until it reaches a maximum at about 25 eV above E_F. The absence of peaks in the DOS near E_F makes it difficult to determine precisely the threshold energy. A more detailed comparison between experiment and theory can be made for the p DOS of Si, which presents a more complex structure, essentially due to hybridized s and p bands.

TABLE I. Broadening widths for the different transitions. Γ_{expt} and Γ_{core} are in eV. C_b is an adimensional parameter which determines the broadening width for band states according to Eq. (6). For $L_{2,3}$ edges, Γ_{core} is slightly different for $2p_{1/2}$ and $2p_{3/2}$ initial core states but we neglect this difference.

| | Edge | Broadening (eV) | | |
		Γ_{inst}	Γ_{core}	C_b
$CoSi_2$	Co K	1.3	1.33	0.05
	Co $L_{2,3}$	0.9	0.43	0.40
	Si K	0.7	0.48	0.03
	Si $L_{2,3}$	$\cdots$	0.015	$\cdots$
$NiSi_2$	Ni K	1.6	1.44	0.05
	Ni $L_{2,3}$	0.3	0.50	0.40
	Si K	0.7	0.48	0.03
	Si $L_{2,3}$	$\cdots$	0.015	$\cdots$

E. Broadening

In order to compare the computed spectra with experiment, it is necessary to take into account different broadening mechanisms. The lifetime of the core hole produces an important broadening, especially for metal K edges. The corresponding broadening width Γ_{core} is inversely proportional to the core-hole lifetime. This broadening is Lorentzian and its width for the different core levels of various elements is tabulated.[35] Another phenomenon which leads to a Lorentzian broadening is the short lifetime of the excited band state. The associated width Γ_{band} depends upon energy.[36] We assumed this dependence to be linear, an approximation which is often made in the XANES range:[27,28]

$$\Gamma_{band}(E) = C_b(E - E_F) . \tag{6}$$

For $L_{2,3}$ edges, the broadening of the L_2 and L_3 spectra have to be carried out separately since these spectra are separated by the spin-orbit energy. After convoluting the spectra with a Lorentzian broadening function of width $\Gamma(E) = \Gamma_{core} + \Gamma_{band}$, we proceed to a Gaussian convolution whose width Γ_{inst} corresponds to the instrumental resolution. The different broadening widths are found in Table I.

IV. RELAXATION EFFECTS

To calculate the absorption spectra we started with the BS obtained within LDA approximation. Our approach for XAS assumes that the absorption is essentially a single-particle process. A step to account for many-body relaxation within the frame of self-consistent LDA band theory is to extract a $1s$ core electron (K edge) or a $2p_{3/2}$ electron (L_3 edge). This extracted electron is then added to the valence electrons. The BS is carried out self-consistently under these conditions. After the system has relaxed, the energies of the different atomic core levels undergo important shifts, as can be seen from Table II

TABLE II. Energy of Co and Si core levels in CoSi$_2$. All energies are relative to $E_F = 0$. These energies are obtained from SCF calculations where the extracted core electron has been added to the valence electrons.

| Core levels | | Energy of core levels in CoSi$_2$ (eV) | | | |
		$1s$	$2s$	$2p_{3/2}$	$2p_{1/2}$
Si without core hole		-1773.18	-133.61	-90.25	-90.89
Si*	$1S$ hole	-1913.55	-159.69	-119.53	-120.38
	$2P_{3/2}$ hole	-1801.89	-151.56	-109.32	-110.02
Co without core hole		-7567.56	-889.50	-756.98	-771.76
Co*	$1S$ hole	-7870.16	-848.19	-828.20	-844.96
	$2P_{3/2}$ hole	-7638.25	-923.37	-796.77	-812.10

for the case of CoSi$_2$. The described procedure to include relaxation has already been applied.[28,38-39]

The XAS including relaxation effects is obtained following the approach of Sec. III B i.e., as the product of the relaxed DOS by the matrix element. The matrix element itself is computed for the situation where the absorbing atom is ionized. This atom is treated as an impurity. In order to allow for more complex symmetry breaking during relaxation, we performed supercell calculations. The residual interactions between ionized atoms can be suppressed if the distance between two ionized atoms is large enough, i.e., if the cell is large enough. However, as will be shown later, it is not important (for the excitations studied here) to perform large supercell calculations. The reason is that the excited electron is attracted to the core hole and remains localized. We also tested the effect of keeping the photoelectron at different energies above E_F (up to 2 Ry) to see if it stays localized on the ionized atom. At every iteration of our self-consistent calculation we placed one electron at the desired energy according to the DOS at this energy. The

self-consistent BS obtained by this procedure showed that the electronic charge distribution in the elementary cell is practically independent of the energy of the photoelectron. In Table III, we show the amount of valence charge localized in the WS sphere surrounding every atom. The calculations show that the additional valence charge is completely localized on the ionized site. Our finding for the excitations studied here is that the photoelectron remains localized within the WS sphere of the excited atom. This is consistent with scattering calculations, where the photoelectron, after having been scattered by neighboring atoms, returns to the ionized site.[40] This situation is the most favorable for minimizing the total energy.

Another test of our method is the calculation of threshold energies. Threshold values have been experimentally determined with a precision of the order of 1 eV. A rough estimation of the threshold energy is given by the difference between core state energies and the Fermi energy. These values are considerably improved by considering the total-energy difference between the nonper-

TABLE III. Valence charge distribution within a unit cell of CoSi$_2$ and NiSi$_2$. Charges are expressed in electrons. Co*, Ni*, and Si* are the ionized atoms for the SCF calculations with a core hole. The comparison of the charge distributions with and without the core hole shows where the photoelectron localizes.

| | | WS spheres | CoSi$_2$: elementary unit cell | | | |
			Co$^{(*)}$	Si$^{(*)}$	Si	Empty
		No core hole	9.47	3.51	3.51	0.50
Valence	Si*	$1S$ hole	9.45	4.59	3.49	0.47
charge		$2P_{3/2}$ hole	9.50	4.59	3.53	0.48
localized	Co*	$1S$ hole	10.50	3.50	3.50	0.49
in each		$2P_{3/2}$ hole	10.51	3.50	3.50	0.50
sphere						

| | | WS spheres | NiSi$_2$: elementary unit cell | | | |
			Ni$^{(*)}$	Si$^{(*)}$	Si	Empty
		No core hole	10.50	3.51	3.51	0.48
Valence	Si*	$1S$ hole	10.46	4.60	3.48	0.47
charge		$2P_{3/2}$ hole	10.50	4.49	3.52	0.48
localized	Ni*	$1S$ hole	11.42	3.54	3.54	0.51
in each		$2P_{3/2}$ hole	11.41	3.54	3.54	0.51
sphere						

turbed state and the relaxed cell calculation. This method to compute threshold energies has already been used for $CoSi_2$ (Ref. 28) and $NiSi_2$.[28,41]

This way to account for relaxation effects is related to the so-called final-state rule (FSR). The FSR approach was developed to treat the excitation problem in the general frame of many-body theory.[38,42–45] This approach permits us to evaluate the effect of the static core hole.[38,42] According to the FSR, the band states have to be calculated with the potential of the final state, i.e., with the core hole included. The effect of using the final-state potential is important when considering the DOS spectra. The main effect is a downward shift and a narrowing of the partial DOS of the ionized atom. However, this effect is very drastic in the case of $CoSi_2$ and $NiSi_2$, and the absorption spectra calculated with the FSR are only improved near the edge. The validity of the FSR for the different types of materials is still uncertain.

Finally, it should be noted that we performed spin-polarized (SP) calculations for both $CoSi_2$ and $NiSi_2$. For the unperturbed state, the application of Stoner's criterion indicates that these materials are far from being magnetic. Nevertheless, when a core electron is extracted from a $1s$ state, the spin of the remaining electron induces magnetization. We applied the formalism described in Sec. III, but with the introduction of the spin as a new quantum number. The valence states are polarized by the core hole, and due to self-consistency the system can relax to a lower total energy than if no spin polarization is allowed. Usually some spin polarization is induced in the valence with a small total moment.

V. RESULTS AND DISCUSSION

A. Threshold energies

From Table IV, we see that the rough estimation of the threshold energies given by the nonrelaxed BS is much too low. This is easily understood since the $1s$ and $2p_{3/2}$ core holes strengthen the attractive potential of the nucleus, since we may represent the core hole by a positive charge. Not surprisingly, it is seen that the unrelaxed calculations give relatively large errors for the light element Si. Here one out of 10 core electrons is extracted,

while in the heavier Ni and Co there are only one out of 18 core electrons. It also appears that the deep levels (K) give the relatively smallest errors in the unrelaxed calculations. This can be understood from the small spatial extent of these states that leads to smaller overlap with the valence states, which in turn leads to a less drastic relaxation of the valence.

From Table III, we see that the energy of a given core level relative to E_F (without a hole) which corresponds to the unrelaxed threshold energy is much lower than the relaxed value. If we perform a self-consistent-field (SCF) calculation where an atom is ionized, the energy of the ionized core level relative to E_F is higher than the relaxed threshold value. In fact, the relaxed threshold values follow the empirical rule found by Liberman[46] in the case of atomic ionization energies:

$$\Delta SCF_c \cong \tfrac{1}{2}(\varepsilon_c^* + \varepsilon_c) , \tag{7}$$

where ΔSCF_c is the relaxed threshold value obtained as the SCF total-energy difference between the systems with and without a core hole, respectively. The values ε_c^* and ε_c are the energies of the ionized and unperturbed core levels, respectively. A theoretical justification for this rule has been derived by Hedin and Johansson.[39] They showed that the SCF total-energy difference between an atom with all core electrons and the atom where core electron c is extracted is approximated to first order by

$$\Delta SCF_c \cong \varepsilon_c + \tfrac{1}{2}\langle c|V_p|c \rangle . \tag{8}$$

The first term ε_c is the energy of core level c, which is the ionization energy according to Koopmans' theorem. The second term is the polarization energy obtained by evaluating the polarization potential in the empty core state c. V_p describes the change in potential due to the polarization of all orbitals when a core electron is extracted. It can be easily shown[39] that a good estimate of the polarization energy is given by

$$E_p = \tfrac{1}{2}\langle c|V_p|c \rangle \cong \tfrac{1}{2}(\varepsilon_c^* - \varepsilon_c) . \tag{9}$$

This approximation for the polarization energy is compatible with Liberman's empirical rule for the threshold energies. In Table V we show values of the polarization

TABLE IV. Threshold energies in eV for K and $L_{2,3}$ edges. The first column corresponds to the unrelaxed threshold value. ΔSCF_c is the SCF total-energy difference between a standard calculation and a calculation with relaxation due to the core hole. $SP - \Delta SCF_c$ is the same as before where the SCF calculations are spin polarized. The last column shows experimental threshold values.

	Edge	$(E_F - \varepsilon_c)$	ΔSCF_c	$SP - \Delta SCF_c$	Expt.
$CoSi_2$	Co K	7567.6	7719.8	7692.2	7706
	Co L_3	757.0	776.8	784.9	777
	Si K	1773.2	1844.1	1829.1	1835
	Si L_3	90.3	100.3	99.5	99.4[a]
$NiSi_2$	Ni K	8187.0	8344.9	8316.1	8330
	Ni L_3	832.1	852.4	850.0	852
	Si K	1773.9	1844.4	1829.3	1835
	Si L_3	91.0	100.7	99.7	99.9[a]

[a]Experimental values taken from Jia et al. (Ref. 20).

TABLE V. ε_c is the energy of the $1s$ or $2p_{3/2}$ core states with all core electrons included. E_p is an estimate of the polarization energy from Liberman's empirical rule. E_t is the threshold energy given by the sum of the unperturbed core state energy and the polarization energy due to the core hole. $\varepsilon^*_{c\,1/2}$ is the energy of the $1s$ core level according to Slater's transition-state rule which is a good approximation of the ΔSCF_c value. ΔSCF_c is the threshold value determined from the SCF total-energy difference. The last column shows experimental values.

		Polarization and threshold energies in CoSi₂ (eV)					
		ε_c	$E_p = 1/2(\varepsilon^*_c - \varepsilon_c)$	$E_t = \varepsilon_c + E_p$	$\varepsilon^*_{c\,1/2}$	ΔSCF_c	Expt.
Si*	$1S$ hole	1773.18	70.19	1843.37	1843.8	1844.1	1835
	$2P_{3/2}$ hole	90.25	9.54	99.79		100.3	99.4
Co*	$1S$ hole	7567.56	151.30	7718.86	7720.0	7719.8	7706
	$2P_{3/2}$ hole	756.98	19.90	776.88		776.8	777

energies for the different core holes. We see that the threshold values obtained by using the ΔSCF method are well approximated by the sum of a core-level eigenvalue and a polarization energy. Another method to approximate the ΔSCF method consists in removing not one but one-half electron from the core. As seen from Table V for the K edges, the obtained eigenvalue energy is a remarkably good approximation to the ΔSCF energy, as predicted by the transition-state rule.[47] This rule, first established by Slater for the $X\alpha$ potential, has been generalized by Janak[48] and by Williams and Lang.[49]

However, as our threshold values are too high, especially for K edges, the reason could lie in an overestimate of the polarization energy. The theory of Hedin and Johansson applies well for deep core levels. For such levels, the contributions to the polarization energy come essentially from the outer electron shells rather than from inner or intra shell contributions. As the atoms are embedded in the solid, the outer valence electrons are more delocalized than in a pure atomic case. This can lead to a noticeable change in polarization energies.

Thus it seems that most of the relaxation can be understood as an atomic process. However, the chemical environment plays some role. For instance, a free-atom calculation of the polarization energy for a $1s$ Si core hole is 70.2 eV; from the CoSi₂ calculation we obtain also 70.2 eV, while in the calculation on TiSi₂ by Czyzyk and de Groot one deduces 65.3 eV.

Our calculated threshold energies agree quite well with the experimental values, as seen From Table IV. However, in general, values from the nonpolarized calculation are slightly too large, while the spin-polarized calculations are slightly too small, indicating a too relaxed configuration. This small discrepancy may come from the fact that local-spin-density (LSD) potentials have been used in all cases, although we know that the exchange due to a partly filled core orbital should be modified.

B. K edges

Figure 4(a) shows the superimposed experimental spectra for CoSi₂ and NiSi₂ Si K edges. They have been adjusted in order to match the edges in the range 2–5 eV above E_F. The origin was chosen to be zero at the Co threshold. The first peak labelled a, in CoSi₂, disappears in NiSi₂. The next peak b, is found in both spectra as well as peak c. These features are well reproduced by the p DOS of the two compounds as is seen in Fig. 4(b). The unoccupied states close to the Fermi level are essentially of p symmetry. The Fermi level in CoSi₂ cuts the tail of this high p DOS structure, whereas in NiSi₂ E_F lies at a relative minimum, making the a peak disappear. In Fig. 5(a), the metal K edges of both Co and Ni show the same trend. The band which is filled when adding an electron to CoSi₂ produces a peak close to E_F in CoSi₂, while this
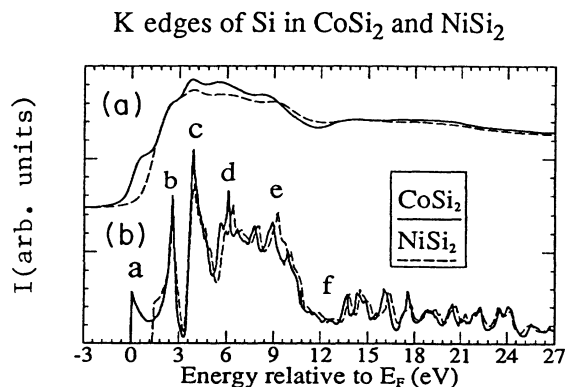

FIG. 4. (a) Superimposed experimental Si K edges of CoSi₂ and NiSi₂. (b) Superimposed p DOS of Si in both disilicides. The energy scale is relative to $E_F = 0$ eV.
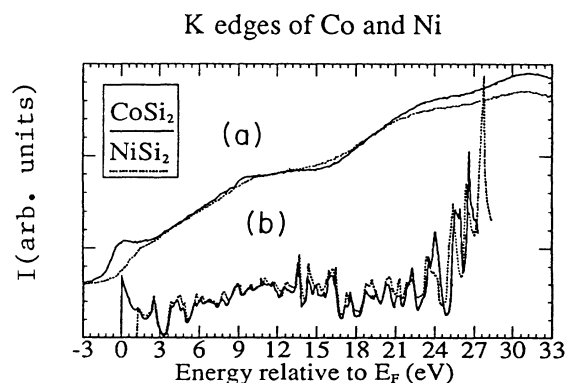

FIG. 5. (a) Superimposed experimental Co and Ni K edge spectra. (b) Superimposed Co and Ni p DOSs. The energy scale is relative to $E_F = 0$ eV.
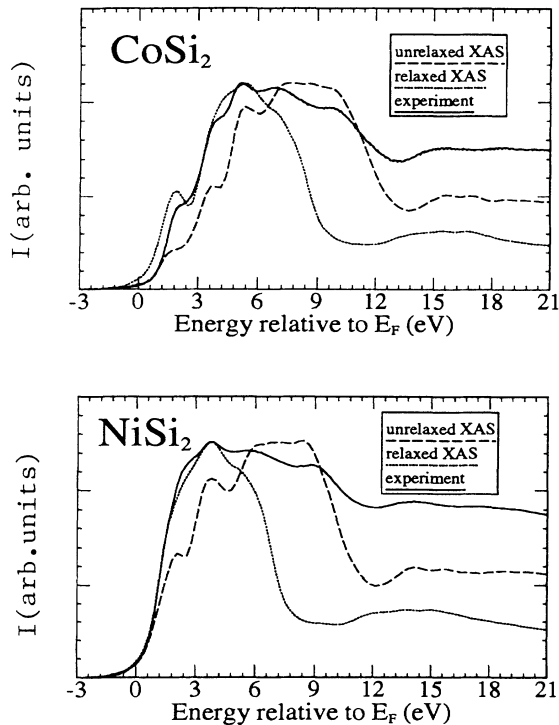
FIG. 6. Calculated relaxed and unrelaxed XAS (including matrix elements and broadening) compared with experimental spectra for Si K edges in $CoSi_2$ and $NiSi_2$.
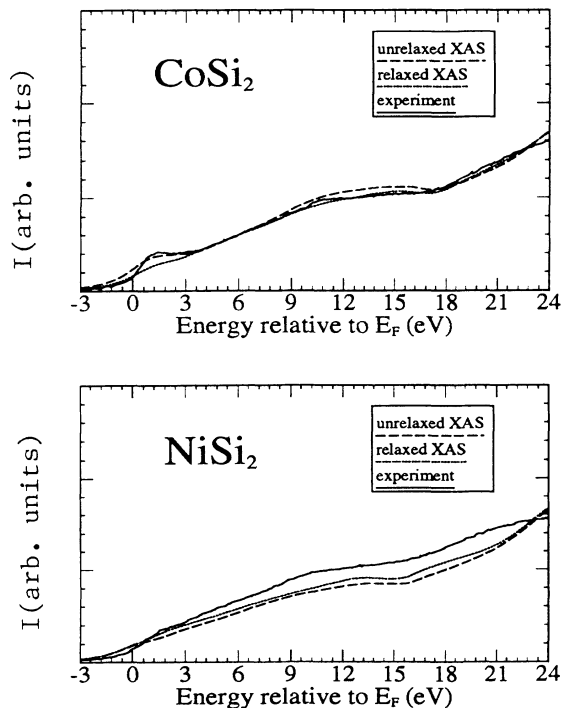
FIG. 7. Calculated relaxed and unrelaxed XAS (including matrix elements and broadening) compared with experiment for the Co and Ni K edges.
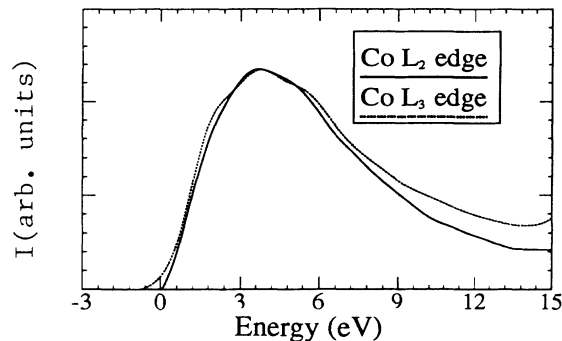
FIG. 8. L_2 and L_3 spectra for Co. The tail of the L_3 contribution has been substracted from the L_2 spectra. Both spectra have been adjusted to the same threshold energy and scaled to the same intensity.

peak is lost in $NiSi_2$, as seen in Figs. 4(a) and 5(a).

Thus the difference between both compounds consists essentially of a shift of E_F to accommodate the extra electron of the metal atom in $NiSi_2$. The comparison between calculated and experimental spectra for the Si K edges is shown in Fig. 6. For the unrelaxed calculation, the intensities are not well described near the edge. The difference with experimental spectra suggests an enhancement mechanism of the DOS near E_F. As seen from Fig. 6, the relaxed curve matches the experiment in a 5 eV range near the threshold. Relaxation produces the desired enhancement of the DOS, but it also drastically reduces its width. It seems that a superposition of the two calculations would better correspond to the experimental spectra. However, calculations of the spectra according to the transition state are close to the relaxed spectra and do not change the results.

The Co and Ni K edges, with and without relaxation, are compared to experiment in Fig. 7. Concerning the shape of the spectra, both calculations give good agreement with experiment.

C. $L_{2,3}$ edges of Co and Ni

The separation between L_3 and L_2 peaks corresponds very closely to the spin-orbit (SO) coupling. The experi-
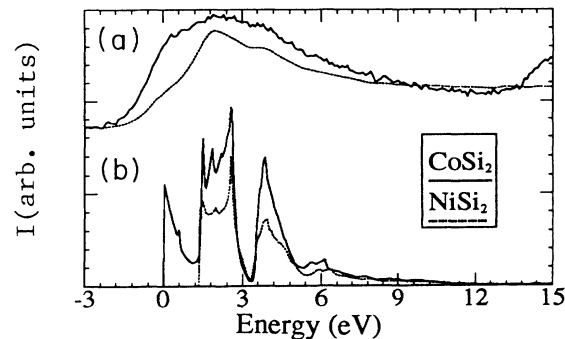
FIG. 9. (a) Superimposed experimental Co and Ni L_3 edge spectra. (b) Superimposed d DOS of Co and Ni. The energy scale is relative to $E_F = 0$ eV.
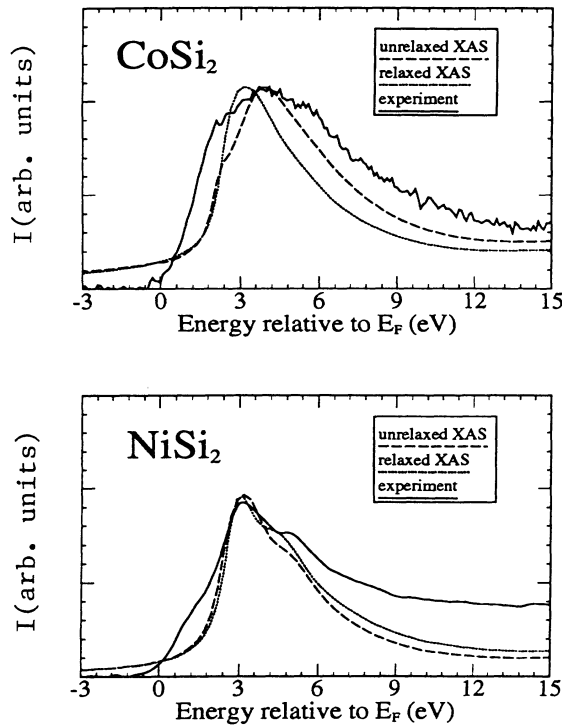
FIG. 10. Calculated relaxed and unrelaxed XAS (including matrix elements and broadening) compared with experiment for the Co and Ni L_3 edges.

mental values determined from the spectra for SO in CoSi$_2$ are 14.8 and 17.4 eV, while the calculations give 14.78 and 17.44 eV, respectively. In Fig. 8, the L_2 and L_3 spectra have been adjusted and scaled to the same intensity. The L_2 edge possesses a too high intensity. The L_3-to-L_2 intensity ratio is close to two, if one subtracts the L_3 contribution (which goes as a λ^3 power law, where λ is the wavelength of the incident beam) in the L_2 range.

In Fig. 9(a), the L_3 absorption spectra for CoSi$_2$ and NiSi$_2$ are superimposed. In Fig. 9(b), both L_3 spectra are shown without broadening. Again, we observe a peak close to E_F for the Co L_3 edge which is lost in the Ni L_3

edge. Finally, in Fig. 10, we compare relaxed and unrelaxed Co and Ni L_3 edges to the experimental spectra.

VI. CONCLUSIONS

In this paper we have given both an experimental and theoretical picture of the K and $L_{2,3}$ edges in CoSi$_2$ and NiSi$_2$. Good agreement has been found between experience and a band-structure approach, for the positions of the different peaks in the spectra. The effect of having a core hole on the absorbing site is to make the nucleus more attractive to valence electrons. The tendency is to pull down valence bands and to make bands narrow, which seems to go in the direction of the experimental spectra. However, the relaxed, self-consistent calculation for the Si K edge leads to an enhanced spectra near the edge but produces a too narrow structure compared to experiment. The use of a larger supercell does not change this fact. One possible interpretation is that the very-near-edge range is best described by the relaxed spectra, calculated according to the FSR, while the higher energy range seems to be better described within the unrelaxed approximation.

Our method neglects dynamical effects which may be important for the considered core levels. On the other hand, our method has the advantage of containing highly nonlinear terms for the relaxation energy of the core and valence electrons, whereas dynamical theories contain essentially linear corrections. Calculated threshold energies by using the ΔSCF method are in excellent agreement with experience. The effect of the core hole on threshold energies can be essentially understood as an atomic process, whereas the effect on the form of the spectra depends significantly on the chemical environment.

*Also at Laboratoire d'Utilisation du Rayonnement Electromagnétique, Université de Paris–Sud, Bâtiment 209C, 91405 Orsay CEDEX, France.

[1] O. Bisi and C. Calandra, J. Phys. C 14, 5479 (1981).

[2] D. M. Bylander, L. Kleinman, K. Mednick, and W. R. Grise, Phys. Rev. B 26, 6379 (1982).

[3] J. Tersoff and D. R. Hamann, Phys. Rev. B 28, 1168 (1983).

[4] J. H. Weaver, A. Franciosi, and V. L. Moruzzi, Phys. Rev. B 29, 3293 (1984).

[5] J. Robertson, J. Phys. C 18, 947 (1985).

[6] J. Xu and Y. Xu, Solid State Commun. 55, 891 (1985).

[7] R. S. Gupta and S. Chatterjee, J. Phys. F 16, 733 (1986).

[8] W. R. L. Lambrecht, N. E. Christensen, and P. Blöchl, Phys. Rev. B 36, 2493 (1987).

[9] L. F. Mattheiss and D. R. Hamann, Phys. Rev. B 37, 10 623 (1988).

[10] K. L. Peterson, J. S. Hsiao, D. R. Chopra, and T. R. Dillingham, Phys. Rev. B 38, 9511 (1988).

[11] J. S. Hsiao and K. L. Peterson, Phys. Rev. B 38, 10 911 (1988).

[12] Y.-J. Chang and J. L. Erskine, Phys. Rev. B 26, 4766 (1982).

[13] A. Franciosi, J. H. Weaver, and F. A. Schmidt, Phys. Rev. B 26, 546 (1982).

[14] Y. J. Chabal, D. R. Haman, J. E. Rowe, and M. Schlüter, Phys. Rev. B 25, 7598 (1982).

[15] O. Bisi, C. Calandra, U. del Pennino, P. Sassaroli, and S. Valeri, Phys. Rev. B 30, 5696 (1984).

[16] G. Gewinner, C. Pirri, J. C. Peruchetti, D. Bolmont, J. Derrien, and P. Thirty, Phys. Rev. B 38, 1879 (1988).

[17]W. Speier, E. V. Leuken, J. C. Fuggle, D. D. Sarma, L. Kumar, B. Dauth, and K. H. J. Buschow, Phys. Rev. B **39**, 6008 (1989).

[18]Y. Garreau, P. Lerch, T. Jarlborg, E. Walker, P. Genoud, A. A. Manuel, and M. Peter, Phys. Rev. B **43**, 14 532 (1991).

[19]G. C. F. Newcombe and G. G. Lonzarich, Phys. Rev. B **37**, 10 619 (1988).

[20]J. J. Jia, T. A. Callcott, W. L. O'Brien, Q. Y. Dong, J.-E. Rubensson, D. R. Mueller, D. L. Ederer, and J. E. Rowe, Phys. Rev. B **43**, 4863 (1991).

[21]H. Nakamura, M. Iwami, M. Hirai, M. Kusaka, F. Akao, and H. Watabe, Phys. Rev. B **41**, 12 092 (1990).

[22]J. F. Van Acker, P. J. Weijs, W. Speier, J. C. Fuggle, and R. Zeller, in *Conference Proceedings of the Second European Conference on Progress in X-Ray Synchrotron Radiation Research,* edited by A. Balerna, E. Bernieri, and S. Mobilio (Italian Physical Society, Roma, 1989), Vol. 25, p. 55.

[23]J. Goulon, M. Lemonnier, R. Cortès, A. Retournard, and D. Raoux, Nucl. Instrum. Methods **208**, 625 (1983).

[24]E. Bouisset, J. M. Estéva, R. C. Karnatak, J. P. Connerade, A. M. Flank, and P. Lagarde, J. Phys. B **24**, 1609 (1991).

[25]C. R. Natoli and M. Benfatto, J. Phys. (Paris) Colloq. **47**, C8-11 (1986).

[26]D. A. Goodings and R. Harris, J. Phys. C **2**, 1808 (1969).

[27]T. Jarlborg and P. O. Nilson, J. Phys. C **12**, 265 (1979).

[28]M. T. Czyzyk and R. A. de Groot, in *Conference Proceedings of the Second European Conference on Progress in X-Ray Synchrotron Radiation Research* (Ref. 22), p. 47.

[29]O. K. Andersen, Phys. Rev. B **12**, 3060 (1975); G. Arbman and T. Jarlborg, J. Phys. F **7**, 1635 (1977).

[30]W. Kohn and L. J. Sham, Phys. Rev. **140**, A1133 (1965).

[31]L. Hedin, B. I. Lundqvist, and S. Lundqvist, Solid State Commun. **9**, 537 (1971).

[32]R. W. G. Wyckoff, *Crystal Structures,* 2nd ed. (Krieger, Malabar, FL, 1982), Vol. I, p. 2493.

[33]O. Jepsen and O. K. Andersen, Solid State Commun. **9**, 1763 (1971).

[34]J. E. Müller and J. W. Wilkins, Phys. Rev. B **29**, 4331 (1984); J. E. Müller, O. Jepsen, and J. W. Wilkins, Solid State Commun. **42**, 365 (1982).

[35]M. O. Krause and J. H. Oliver, J. Phys. Chem. Ref. Data **8**, 329 (1979).

[36]I. Lindau and W. E. Spicer, J. Electron Spectrosc. Relat. Phenom. **3**, 409 (1974).

[37]E. J. Mele and J. J. Ritsko, Phys. Rev. Lett. **43**, 68 (1979).

[38]U. von Barth and G. Grossmann, Solid State Commun. **32**, 645 (1979).

[39]L. Hedin and A. Johansson, J. Phys. B **2**, 1336 (1969).

[40]Ph. Sainctavit, J. Petiau, M. Benfatto, and C. R. Natoli, in *Conference Proceedings of the Second European Conference on Progress in X-Ray Synchrotron Radiation* (Ref. 22), p. 31.

[41]W. R. L. Lambrecht, Phys. Rev. B **34**, 7421 (1986).

[42]L. Hedin, J. Phys. (Paris) Colloq. **39**, C4-103 (1978).

[43]P. H. Citrin, G. K. Wertheim, and M. Schlüter, Phys. Rev. B **20**, 3067 (1979).

[44]U. von Barth and G. Grossmann, Phys. Rev. B **25**, 5150 (1981).

[45]C. A. Almbladh and U. von Barth, Phys. Rev. B **13**, 3307 (1976).

[46]D. Liberman, Bull. Am. Phys. Soc. **9**, 731 (1964).

[47]J. C. Slater, *The Self-Consistent Field for Molecules and Solids* (McGraw-Hill, New York, 1974), Vol. 4, p. 35.

[48]J. F. Janak, Phys. Rev. B **18**, 7165 (1978).

[49]A. R. Williams and N. D. Lang, Phys. Rev. Lett. **40**, 954 (1978).